




Article

Exploring the Potential of Soil Salinity Assessment through Remote Sensing and GIS: Case Study in the Coastal Rural Areas of Bangladesh

Billal Hossen ^{1,2} , Helmut Yabar ^{1,*}  and Md Jamal Faruque ³ 

¹ Graduate School of Life and Environmental Sciences, University of Tsukuba, 1-1-1 Tennodai, Tsukuba 305-8572, Japan

² Department of Agricultural Extension, Khamarbari, Farmgate, Dhaka 1215, Bangladesh

³ Bangladesh Agricultural Development Corporation (BADDC), Dhaka 1000, Bangladesh

* Correspondence: yabar.mostacero.h.ke@u.tsukuba.ac.jp; Tel.: +81-29-853-4269

Abstract: Soil salinity is a negative impact of climate change, and it is a significant problem for the coastal region of Bangladesh, which has been increasing in the last four decades. The issue of soil salinity substantially limits the agricultural crop production in coastal areas. Therefore, a soil salinity assessment is essential for proper land-use planning in agricultural crop production. This research was carried out to determine the soil salinity area with different salinity levels in Barguna Sadar Upazila (sub-district). The remote sensing technique, which is a potentially quick yet effective method for the soil salinity estimation in data-scarce conditions, was applied. The methodology employed the Landsat 8 OLI dataset along with nine soil salinity indices to develop a soil salinity map. The maps were from Soil Resource Development Institute (SRDI), and low NDVI value (−0.01 to 0.48) was produced using satellite images illustrate the extent of the soil salinity for the study area. However, nine linear regressions, which were made between the pixel value of the satellite-based generated map and ground truth soil salinity data, that is, the EC value, indicate a maximum R^2 value for the salinity index $SI_7 = G \times R/B$, representing a value of 0.022. This minimal R^2 value indicates a negligible relationship between the ground EC value and the pixel value of the salinity index generated map, inferring that the indices are not sufficient to assess the soil salinity. Nonetheless, this research's findings offer a guide for researchers to investigate alternative geospatial approaches for this geophysical condition.

Keywords: soil salinity; coastal region; remote sensing; electrical conductivity; salinity index



Citation: Hossen, B.; Yabar, H.; Faruque, M.J. Exploring the Potential of Soil Salinity Assessment through Remote Sensing and GIS: Case Study in the Coastal Rural Areas of Bangladesh. *Land* **2022**, *11*, 1784. <https://doi.org/10.3390/land11101784>

Academic Editor: Purushothaman Chirakkuzhyil Abhilash

Received: 6 September 2022

Accepted: 10 October 2022

Published: 13 October 2022

Publisher's Note: MDPI stays neutral with regard to jurisdictional claims in published maps and institutional affiliations.



Copyright: © 2022 by the authors. Licensee MDPI, Basel, Switzerland. This article is an open access article distributed under the terms and conditions of the Creative Commons Attribution (CC BY) license (<https://creativecommons.org/licenses/by/4.0/>).

1. Introduction

Bangladesh's coastal areas are hydrologically and geomorphologically dominated by the Bay of Bengal and Ganges Brahmaputra Meghna (GBM) river system. The coastal zone covers 47,201 km², or 32 percent of the country's surface, and it comprises 19 districts. The coastal area accommodates 35 million people or 29% of the country's population. Jessore, Narail, Gopalganj, Shariatpur, Chandpur, Satkhira, Khulna, Bagerhat, Pirozpur, Jhalakati, Barguna, Barisal, Patuakhali, Bhola, Lakshmipur, Noakhali, Feni, Chittagong, and Cox's Bazar comprise the 19 coastal districts of Bangladesh [1,2]. Bangladesh is one of the most vulnerable countries to the impacts of climate change. Various natural disasters and hazards, including intense rainfall, cyclones, regular flooding, thunderstorms, tornadoes, storm surges, salinity intrusion, and others, have become predominant in this country, and the intensity of these disasters has been rising in the coastal regions [3,4].

The most common and potential effect of climate change includes sea-level rise which causes the inundation of low-lying areas, the development of soil salinity which is caused by saltwater intrusion, and wetland loss. Globally, roughly 600 million residents in the coastal low-elevation regions are impacted by growing salinization [5,6]. According to

recent studies, the sea levels may rise by one meter or more during the twenty-first century and this is linked to climate change, thereby leading to adverse impacts on one billion people by 2100 [7–12]. Bangladesh is one of the nations that is most at risk from a predicted sea-level increase which is induced by climate change. In addition, many studies assert that climate change alarmingly raises the level of the soil salinity in coastal Bangladesh [13–15].

Due to the entrance of saltwater, agricultural cropland is severely affected, thereby reducing the agrarian crop production rates. Mangrove forests and fisheries of the coastal zone are also at risk of incurring damage from salinization [15–20]. Because of its remarkable effects on agriculture, coastal ecosystems, infrastructure, aquaculture, and the availability of fresh water for domestic and commercial usage, rising salinity from saltwater intrusion that is caused by climate change may be the greatest danger to the livelihoods and public health of coastal inhabitants. Recent studies show that by 2050, climate change could significantly alter the river salinity in Bangladesh’s southwest coastal region [21]. These modifications are anticipated to cause a lack of water for irrigating dry-season crops, considerable alterations in the coastal aquatic ecosystems, and significant drinking water shortages in coastal metropolitan areas [21].

Consequently, understanding soil salinity’s physical and economic implications and planning strategic adaptation measures will be essential for the long-term growth of and poverty reduction in the nations with susceptible coastal regions [12]. Therefore, it is necessary to check and monitor the soil salinity in coastal Bangladesh continuously. This would also help the policymakers and the government to take appropriate measures to address climate change issues to improve public health.

The coastal area accounts for more than 30% of Bangladesh’s cultivable land. These regions’ proximity to the ocean, low-land topography, the meeting of the mighty Ganges, Brahmaputra, and Meghna rivers, decreased upstream freshwater supplies, and delicate agro-ecosystems make them even more sensitive to the effects of climate change. Different soil salinity levels already affect about 37% of the cultivable coastal land [22]. The Soil Resource Development Institute (SRDI), at the Ministry of Agriculture, reported that around 2.86 million hectares of coastal and off-shore land are affected by the varying levels of salinity, including 1.056 million hectares of arable land [22].

In 2009, the current geographic distribution of the saline soils was examined utilizing reconnaissance soil survey techniques and various base materials such as aerial images, a toposheet, Upazila soil, a landform map, a previously published soil salinity map, and so on. Soil salinity affects 1.056 million hectares of coastal land from a total area of 1.689 million hectares. About 0.328, 0.274, 0.189, 0.161, and 0.101 million hectares of land are affected by soil that is very slightly saline (S1), slightly saline (S2), moderately saline (S3), intensely saline (S4), and very strongly saline (S5), respectively. More recently, salinity has affected the land areas in the Barisal Satkhira, Borguna, Pirojpur, Jessore, Jhalakathi, Narail, Patuakhali, Madaripur, and Gopalganj districts, thereby reducing their agricultural production significantly. Table 1 compares the soil salinity in the coastal areas during the last four decades from 1973 to 2009. A comparison of the salt-affected site from 1973 to 2009 has revealed that during the period, over 0.223 million ha (26.7 percent) of new land had been impacted by varying degrees of salinity (Table 2). It was also discovered that throughout the last nine years, from 2000 to 2009, approximately 35,440 hectares of new land had been affected by varying degrees of salinity [22].

Table 1. Soil salinity-affected areas in the coastal region between 1973 and 2009 [22].

The Total Area Affected by Soil Salinity ($\times 10^3$ ha)			Different Soil Salinity Classes and Areas ($\times 10^3$ ha)											
			S1 2.0–4.0 dS/m			S2 4.1–8.0 dS/m			S3 –16.0 dS/m			S4 >16 dS/m		
1973	2000	2009	1973	2000	2009	1973	2000	2009	1973	2000	2009	1973	2000	2009
833.45	1020.75	1056.26	287.37	289.76	328.43	426.43	307.20	274.22	79.75	336.58	351.69	39.90	87.14	101.92

Table 2. Increase in soil salinity salt-affected area from 1973 to 2009 [22].

Period 2000–2009 ($\times 10^3$ ha)	Period 1973–2009 ($\times 10^3$ ha)
35.51 (3.5%)	222.81 (26.7%)

According to the Soil Resource Development Institute (SRDI) [22], the leading causes of increased soil salinity in the topsoils of the coastal region are expected to be as a result of irregular rainfall, the withdrawal of fresh river water from upstream, the faulty management of sluice gates and polders, the introduction of brackish water from shrimp cultivation, the regular saline tidal water flooding of unprotected areas, and the capillary rise of soluble salts.

Soil salinity harms the coastal ecology's health since it affects the soil's health and vegetation. Moreover, it is a significant threat to the growth and development of the plants. Agricultural crop production has been decreasing with the changing of the cropping patterns in coastal areas over the years as a consequence of soil salinity. Plant growth is hampered by salts, which increase the soil osmotic pressure and impede the normal nutrition uptake by plants from the ground. The water deficit or osmotic pressure that is caused by the soil salinity clarifies that salt concentration plays a role in reducing the capacity of a crop plant to uptake the soil water.

Consequently, the plant growth process becomes slow when the soil contains a high salt concentration. Munns et al. also observed that the osmotic effect of soil salinity renders changes in the plant's metabolic process, which often resemble the wilting that is caused by water deficiency [23]. Furthermore, salinity stress inhibits the growth of the plant due to there being imbalances in the nutritional uptake and specific ion toxicity for the plant [24] or a combination of these variables [24,25]. Indeed, the effects of salinity on the plant's growth are time-dependent, which means that the intensity of the salinity effect varies with the growth stage of the plants; Munns et al. devised a two-stage model to demonstrate how the growth stage of plant is affected by salinity [26]. The initial step is rapid, wherein the growth slowing that occurs is attributed to the emergence of the water shortage. The second stage, which is very sluggish, is caused by the accumulation of lethal amounts of salts in the shoot. Flexas et al. observed that salinity impacts photosynthesis by reducing the CO_2 availability due to diffusion constraints and lowering the photosynthetic pigment content [27–30].

Along with the significance of rising soil salinity, soil health, the prime determining factor of crop cultivation in coastal areas, has decreased over the years. Consequently, the soil salinity area determination and the mapping of it could be essential for an appropriate land-use planning and agricultural policy to be made to enhance the crop production.

A soil salinity assessment through a remote sensing analysis using satellite data is very convenient, effective, and sustainable in situations where the field data are scarce. Generally, a soil salinity determination through a field measurement process and a laboratory analysis is time-consuming and expensive; it poses the challenge of an extensive area examination. Thus, a remote sensing analysis could be an innovative problem-solving technique that is used to overcome these constraints for a soil salinity assessment. Traditionally, the measurement of the soil salinity involves the collection of soil samples, their processing, and a laboratory analysis to determine the concentration of the solutes or electrical conductivity (EC). However, these methodologies are expensive and time-consuming since intensive sampling is required to assess the area's geographic variability [31,32]. Ghabour and Daels observed that a soil salinity determination has traditionally taken time [31]. However, the remote sensing methods provide more efficient and cost-effective tools for estimating and mapping the soil salinity. In addition, when it is compared to the conventional methods, the remote sensing technique is faster, and it is easier to create and update the spatial maps with information [32–35]. Integrating remote sensing data and processes with geographic information systems (GIS) is beneficial since GIS displays the spatial distribution of salinity

and its related environmental dangers, and mapping soil salinity has become a simple operation over the past three decades [36–38].

The reflectance that comes from various soil types that are concentrated with multiple degrees of salinity is very sensitive to the electromagnetic spectrum wavelengths in the near-infrared (NIR) to shortwave infrared (SWIR) range [39]. Remote sensing technology has recently become popular for assessing and monitoring the level of soil salinity, as salty soil provides a higher reflectance in the visible and infrared range [32,40,41]. The production of a soil salinity map could be based on estimating a range of soil salinity indicators using the satellite data from Landsat 5, Landsat 7, and Landsat 8 [42]. The remote sensing-based comprehensive land surface factor system (CLSFS) (which comprises four factors—spectral information, the ecological indices, the spatial location, and the land cover) [43] along with CLSFS (comprising—the salinity index, the heat and moisture index, the spectral value, the vegetation index, the spatial location, and the land cover) could achieve the significant result in terms of soil salinity mapping [44].

Observing and identifying the spatial area distribution of the salt-affected area is possible with the use of satellite imagery. Furthermore, satellite data and remote sensing techniques can also likely assess the temporal soil salinity changes and the soil salinity dynamics over the period that is studied. If a model is generated for a particular area, it is possible to use that model to analyze the soil salinity for the other part of the country. Bangladesh's Soil Resource Development Institute (SRDI) performs soil salinity assessments through field surveys and laboratory analyses, which are time-consuming and challenging. Hence, this research aims to determine the spatial and aerial distribution of the land area that is affected by various degrees of soil salinity through remote sensing techniques for the achievement of improved analytical measures.

2. Materials and Methods

2.1. Study Area

The research was carried out in Barghuna Sadar Upazila (sub-district) in the Barguna District, which is situated in the coastal region of Bangladesh, as illustrated in Figure 1. The study area covers 454.39 square kilometers, and it is located between the latitudes 21°58' and 22°15' north and the longitudes of 89°59' and 90°14' east. It is bordered on the north by Betagi, Mirzaganj, and Patuakhali Sadar Upazilas, on the south by the Bay of Bengal and Amtali Upazila, on the east by Patharghata and Bamna Upazilas, and on the west by Patharghata and Bamna Upazilas. Soil salinity is a salient feature in the study area, where most of the land area is highly affected by various degrees of soil salinity. Around 60% of the population is involved in the agriculture sector. The range of crops that growing in this are rice, green gram, groundnut, kheshari, and some vegetables which are the main crops (Barguna Sadar Upazila, Bangladesh National Portal, n.d.9).

2.2. Datasets

Two types of datasets were used in this research.

- (1) Landsat 8 OLI satellite data were used to develop a salinity map which was downloaded from the United States Geological Survey (USGS). The path and row that were used in USGS to download the image are 137 and 44, respectively. The cloud cover was less than 10 percent.
- (2) For the ground truth data, a printed map was collected from the Soil Resource Development Institute (SRDI), Ministry of Agriculture. The map illustrates the various point locations with the soil salinity data and the electrical conductivity (EC) value.

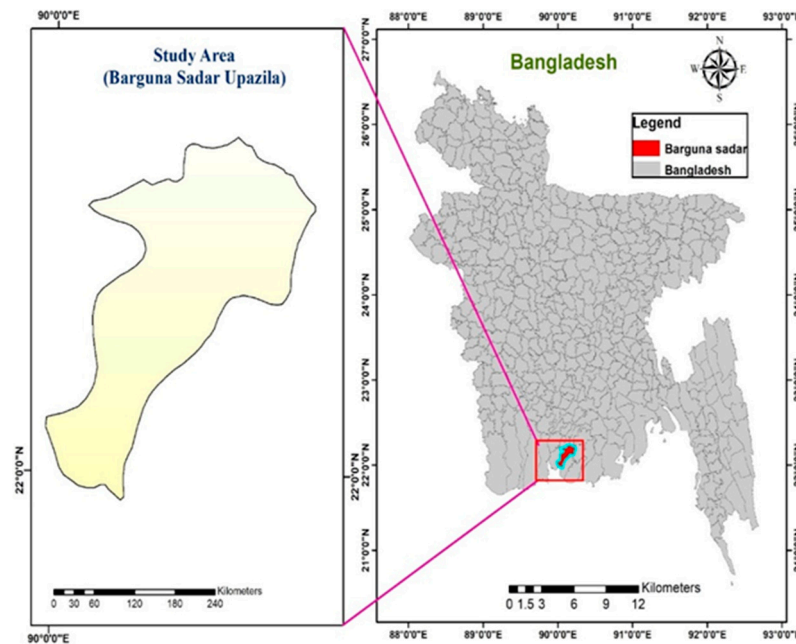


Figure 1. Study area—Barguna Sadar Upazila.

2.3. Methodology

2.3.1. Land Use–Land Cover Classification

The Land Use–Land Cover (LULC) classification was performed for the spatial identification and categorizing the various components of the earth’s surface, such as the vegetation, the agriculture, the water bodies, and the urban areas. The extent of these components also can be determined in hectares from the LULC map. The LULC classification was performed in Google Earth Engine Platform (GEE), a cloud-based computing platform with a machine learning algorithm. GEE is going to be a popular tool for spatial data analysis. According to past studies, GEE has been used in various fields, including agriculture, forestry, economics, and medicine [45,46]. The Landsat 8 datasets that were utilized in assembling the map comprise—the Landsat 8 Collection 1 Tier 1 calibrated top-of-atmosphere (TOA) reflectance with a cloud cover of less than 10% for May 2017. The process began with loading the study area (ROI) and satellite data and clipping the data for the ROI. Then, the training data was collected with the collection of many sample points followed by assembly of all of the sample points. Finally, a smile cart classifier was utilized to classify the image, and an accuracy assessment was performed using a confusion matrix, and a 93.72% accuracy was determined [16]. The final map was exported for its use in the ArcGIS environment to calculate the areas with different classes as per a supervised classification. The entire process followed the Figure 2.

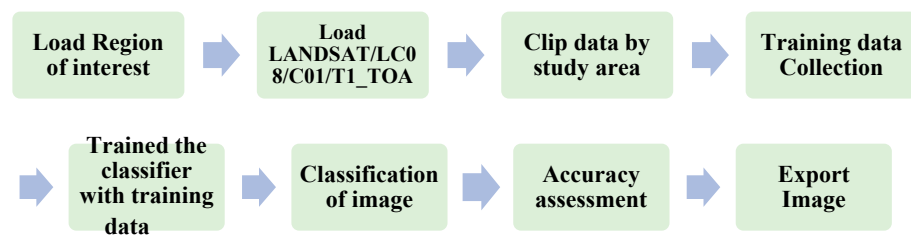


Figure 2. Flow chart for developing Land Use–Land Cover Map.

2.3.2. Normalized Difference Vegetation Index (NDVI)

The normalized differential vegetation index (NDVI) [47] is a widely used indicator that measures the amount and quality of the vegetation on a given ground surface. Studies

have shown that the NDVI can distinguish between the vegetation types, including savannah, dense forest, non-forest, and agricultural fields. Moreover, it determines whether a forest is evergreen or seasonal [48]. It can also be used to estimate a variety of vegetation properties, such as the chlorophyll concentration in leaves [49], the biomass [50], the Leaf Area Index (LAI) [51], the plant productivity [52], the plant stress [53] and the fractional vegetation cover [54].

The value of the NDVI ranges from -1 to $+1$; the higher the NDVI value is, then the higher the vegetation concentration in the landscape is. A negative NDVI index value generally denotes the non-green areas, such as deserts, water, rivers, and built-up regions, whereas a positive number denotes the green areas [55]. The NDVI value can also be used to assess the health condition of plant and vegetation communities. This is due to the expectation that healthy plant communities would have higher NDVI values than unhealthy plants would. The NDVI map was generated using Landsat 8 OLI with 30 m spatial resolution, which was downloaded from <https://earthexplorer.usgs.gov/> in 25 May 2017.

The NDVI was calculated as in Equation (1)

$$\text{NDVI} = \frac{\text{NIR [Band 5]} - \text{RED [Band 4]}}{\text{NIR [Band 5]} + \text{RED [Band 4]}} \quad (1)$$

where NIR [Band 5] and RED [Band 4] represent the near-infrared and the red band of Landsat 8 OLI products, correspondingly.

2.3.3. Satellite Data-Based Soil Salinity Map Preparation and Regression Analysis

The Landsat 8 OLI data was downloaded from Earth Explorer, United States Geological Survey (USGS) (<https://earthexplorer.usgs.gov/>) in 25 May 2017. The path and row were 137 and 44, respectively, with there being less than 10 percent cloud cover. First, atmospheric and radiometric corrections were applied to the Landsat 8 satellite images through ArcGIS 10.7. This preprocessing is performed to lessen the atmospheric perturbations and radiometric distortions that are produced by aerosols, clouds, and other atmospheric particles [56]. The atmospheric correction of the satellite image is necessary to determine the actual surface reflectance value to recover the data accurately as the influence of the absorption of water vapor is substantial for the TM/ETM + near-infrared (IR) channels in the Landsat satellite images [57]. Then, these corrected bands were extracted to obtain the study area using the ‘extract by mask’ function in ArcGIS. Thereafter, the salinity indices were estimated through a raster calculator in ArcGIS to produce a salinity map with different salinity classes (Table 3) based on assigning relevant pixel values to the EC values. Finally, a linear regression analysis was carried out to determine the relationship between the ground EC measurements and the satellite image index values.

Table 3. Five soil salinity classes and their effect on plants [58].

Salinity Class	EC (ds/m)	Level of Salinity Effects on Plants
Non-saline	0–2	Negligible effects on plants.
Slightly saline	2–4	Reduction of crop yield for susceptible plants.
Moderately saline	4–8	Affect a wide variety of plants and limit their yield.
Highly saline	8–16	Only salinity-resistant crops can survive.
Extremely saline	>16	Most of the plants cannot grow up. Only a few highly resistant crops survive.

Nine soil salinity indices were applied to the satellite images from 2017 to develop salinity maps for Barguna Sadar Upazila. These included five salinity classes (non-salty, slightly salty, moderately salty, highly saline, and extremely saline). The salinity indices

that were used to create the maps are listed in Table 4. Accordingly, the nine-soil salinity map was generated based on the satellite data.

Table 4. Various Salinity Indices (SI) used to develop soil salinity map.

Salinity Index (SI)	Description	References
$SI\ 1 = \sqrt{B2 * B4}$	B2 = Blue (Band 2) B4 = Red (Band 4)	[59]
$SI\ 2 = \sqrt{B3 * B4}$	B3 = Green (Band 3) B4 = Red (Band 4)	[59]
$SI\ 3 = \sqrt{(B3)^2 + (B4)^2 + (B5)^2}$	B3 = Green (Band 3) B4 = Red (Band 4) B5 = Near Infrared (Band 5)	[60]
$SI\ 4 = \sqrt{(B3)^2 + (B4)^2}$	B3 = Green (Band 3) B4 = Red (Band 4)	[60]
$SI\ 5 = \sqrt{(B4)^2 + (B5)^2}$	B4 = Red (Band 4) B5 = Near Infrared (Band 5)	[59]
$NDSI = \frac{R - NIR}{R + NIR}$	NDSI = Normalized Differential Salinity Index R = Red, NIR = Near Infrared	[59]
$SI\ 6 = \frac{SWIR-1 * SWIR-2 - SWIR-2 * SWIR-1}{SWIR-1}$	SWIR = Short-Wave Infrared	[61]
$SI\ 7 = \frac{G * R}{B}$	G = Green Band, R = Red Band	[61]
$SI\ 8 = \frac{R * NIR}{G}$	R = Red Band, NIR = Near Infrared, G = Green Band	[62]

The ground truth soil salinity (EC value) data were collected from the Soil Resource Development Institute (SRDI), Ministry of Agriculture, Bangladesh, as a printed map [Figure 3a] showing the 85 locations of the soil sampling points. The soil salinity, which is shown in the printed map, involves examining the soils' physical properties through collecting the soil sample, drying, and estimating the EC values through a laboratory chemical analysis. These data were acquired from April to May 2017. Each point location represents the ground soil salinity and the EC values with various ranges. These field measurements are required to create a relationship between satellite image-derived salinity indices and the field data of the EC value. First, this printed map was scanned, and this step was followed by the digitization one. Next, the digitized map was georeferenced using WGS 1984 UTM 46 N, and lastly, a point shapefile was produced, as shown in Figure 1. All of these processes were carried out using ArcGIS 10.7 software (Esri, Redlands, California, USA; www.esri.com/software/arcgis, accessed on 8 October 2022).

Next, the pixel values from the salinity indices generated map was extracted using the spatial analyst tool for each point of the EC values in the point shape, thereby giving each EC value a unique pixel value. For this purpose, 85 points locations were considered. This process was carried out for all of the salinity indices. It implies that all of the EC values of the point shapefile have corresponding pixel values for all of the indices. Finally, the following linear regression was carried out for all of the salinity indices maps using the obtained EC and the pixel values to observe the relationship between the pixel and the ground EC values. Accordingly, a nine-linear regression chart was generated with the R^2 values. Notably, if there was a good correlation between these values for a specific salinity index, then the salinity map could be produced for different times and places using a specific index calculation.

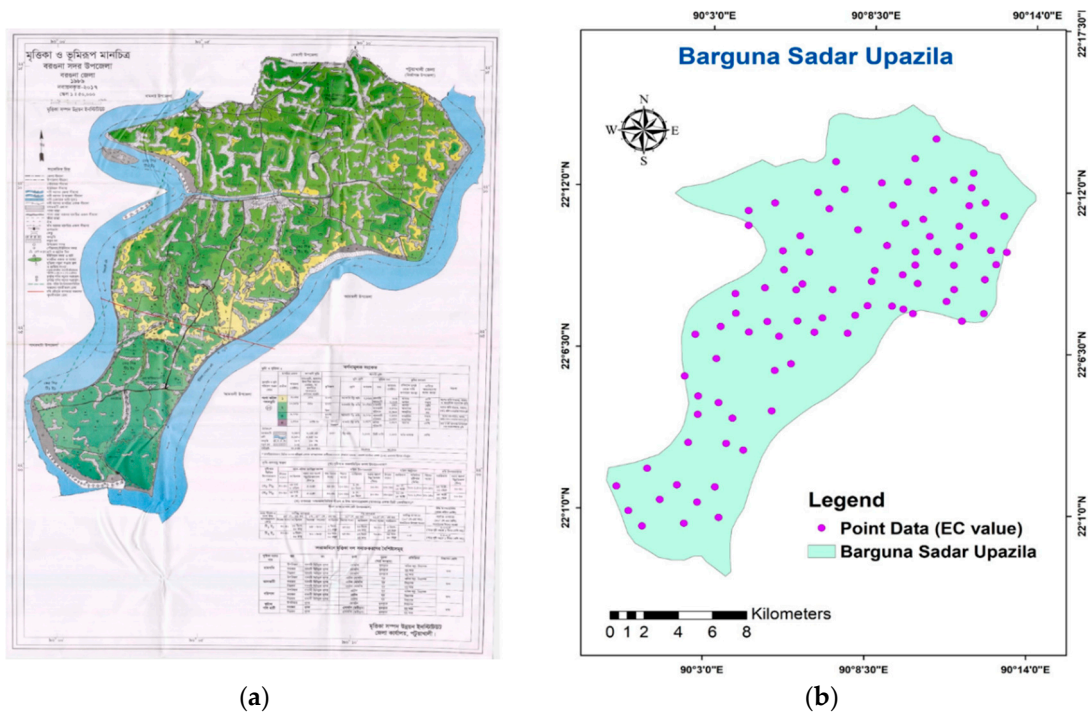


Figure 3. (a) Barguna Sadar Upazila (Sub-district) scanned map; (b) Generated point shapefile for Barguna Sadar Upazila.

3. Results

3.1. Land Use–Land Cover (LULC) Classification

The LULC map classification encompasses five categories: water, forest, agriculture, built environment (which includes urban areas, shores, bare areas, and roads), and villages (comprising homes, trees, and rural roads) (Figure 4). The area of these categories is determined in hectares with the water cover encompassing 7639.02 ha, the forest area encompassing 350.73 ha, the agricultural land encompassing 18,514.53 ha, the built-up area encompassing 3258.63 ha, and the villages encompassing 9657.72 hectares, respectively. Half of the Barguna Sadar represents agricultural land, representing 46.97% of the total area. The other classes contain viz water, forests, built-environments, and villages, occupying 19.38%, 0.89%, 8.27%, and 24.5% of the areas, individually.

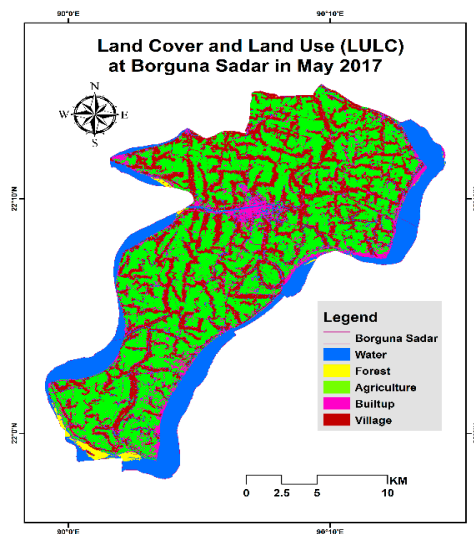


Figure 4. Land Use–Land Cover Classification.

3.2. Normalized Difference Vegetation Index (NDVI)

The NDVI is a vegetation index that is used to calculate the state of the vegetation for a particular area. The NDVI values range from -1 to $+1$, whereby a negative value indicates water and cloud, a positive value with near zero refers to bare land, and a higher value ranges from sparse vegetation (0.1 – 0.5) to dense vegetation (0.6 or above) [47]. It implies that the higher the value of the greenness of the vegetation, then the higher the NDVI value will be. The results from the NDVI map indicate that the value ranges from -0.01 to 0.48 , which is lower than the standard value is. It is also found that the NDVI value for the significant area is much lower than 0.48 , indicating that the site has no or a poor amount of vegetation (Figure 5).

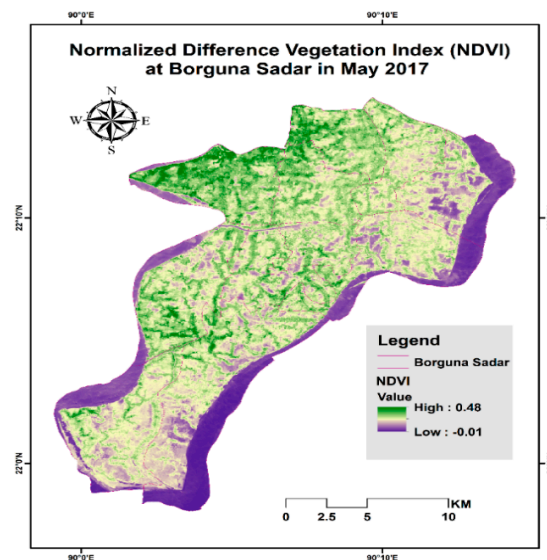


Figure 5. Normalized Difference Vegetation Index (NDVI) map.

3.3. Satellite-Based Soil Salinity Maps and Regression Charts

Nine soil salinity maps were generated using the nine soil salinity indices, which are given below in Figure 6a–i.

The results of the linear regression between the salinity indices value and the corresponding reflectance value are illustrated below in Table 5 and Figure 7.

Table 5. Linear regression analysis results for nine different salinity indices.

Salinity Index (SI)	Index Range	Date of Satellite Image	Number of Samples	R ²
SI 1 = $\sqrt{B2*B4}$	0.095–0.4	25 May 2017	85	0.0208
SI 2 = $\sqrt{B3*B4}$	0.084–0.41	25 May 2017	85	0.021
SI 3 = $\sqrt{(B3)^2 + (B4)^2 + (B5)^2}$	0.17–0.83	25 May 2017	85	0.00006
SI 4 = $\sqrt{(B3)^2 + (B4)^2}$	0.12–0.59	25 May 2017	85	0.0207
SI 5 = $\sqrt{(B4)^2 + (B5)^2}$	0.13–0.72	25 May 2017	85	0.00009
NDSI = $\frac{R-NIR}{R+NIR}$	-0.69 – 0.17	25 May 2017	85	0.0076
SI 6 = $\frac{SWIR1*SWIR2-SWIR2*SWIR1}{SWIR-1}$	0.009–0.099	25 May 2017	85	0.0042
SI 7 = $\frac{G * R}{B}$	0.05–0.44	25 May 2017	85	0.0228
SI 8 = $\frac{R * NIR}{G}$	0.079–0.62	25 May 2017	85	0.0011

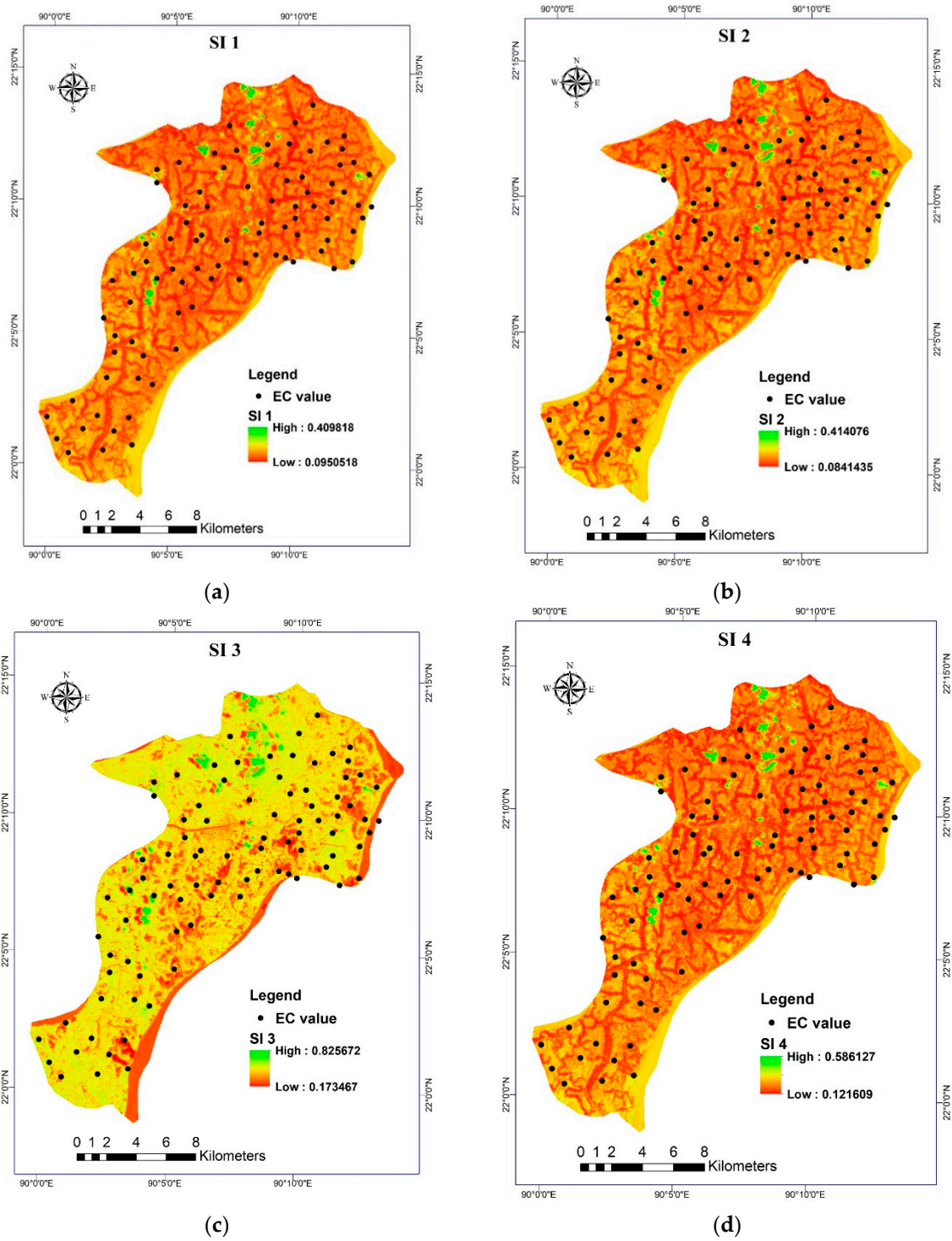


Figure 6. Cont.

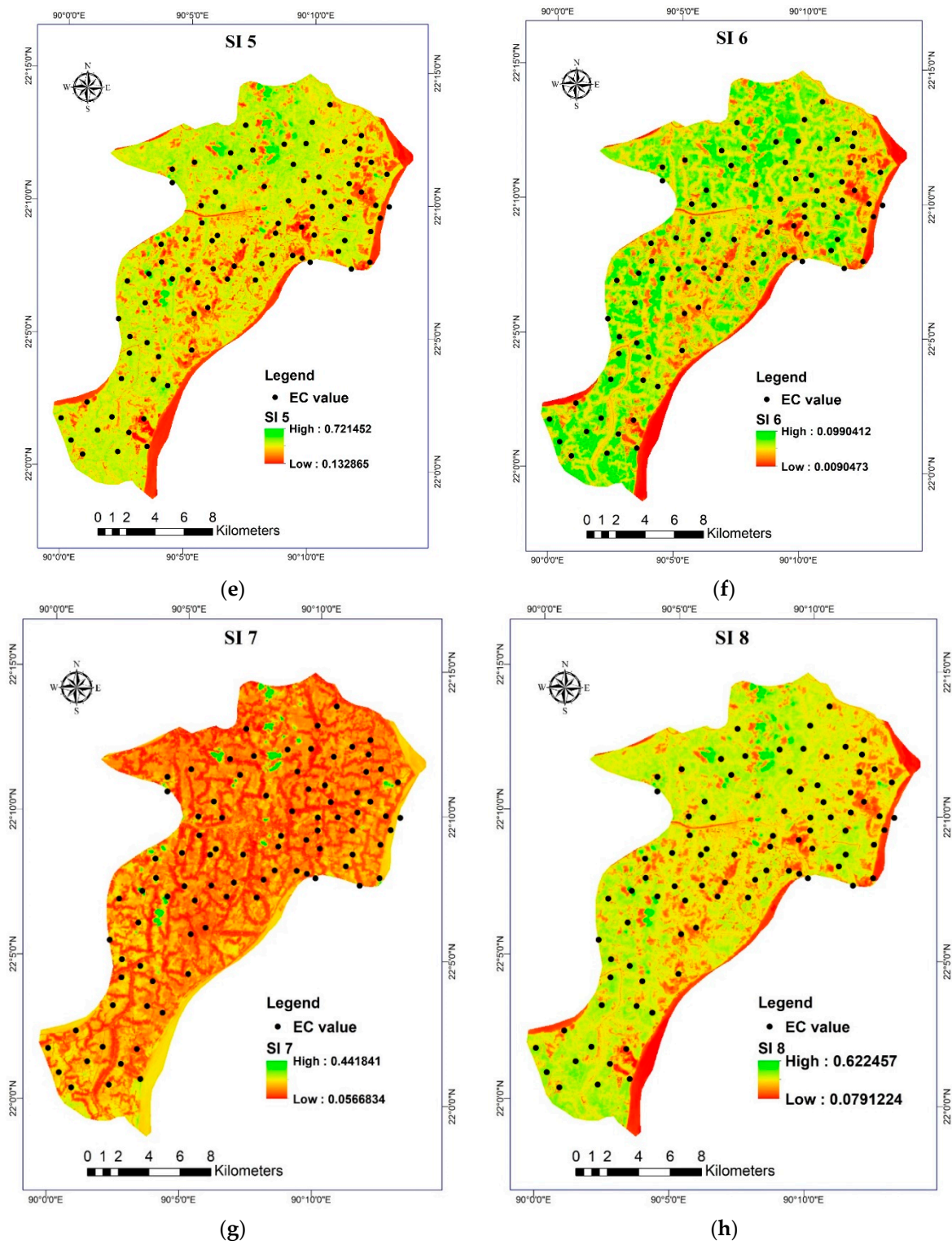
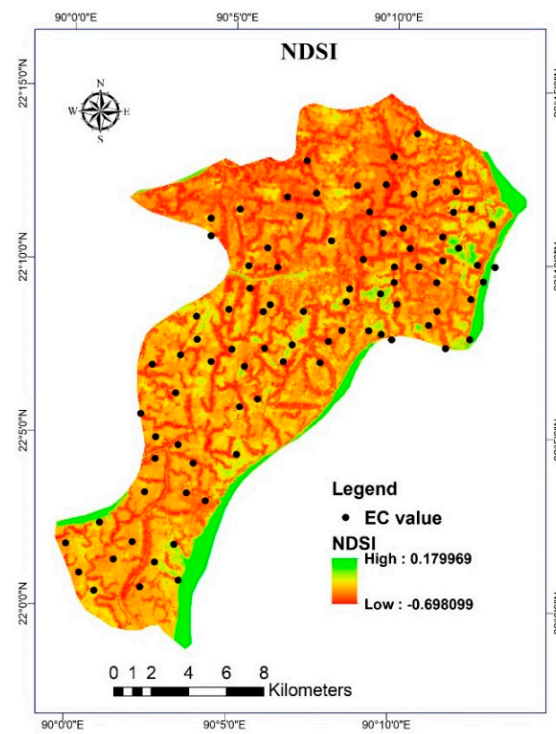
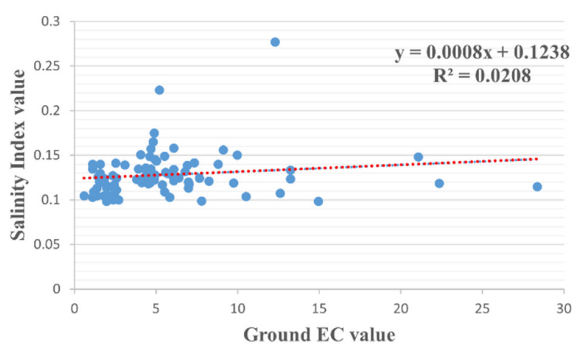


Figure 6. Cont.

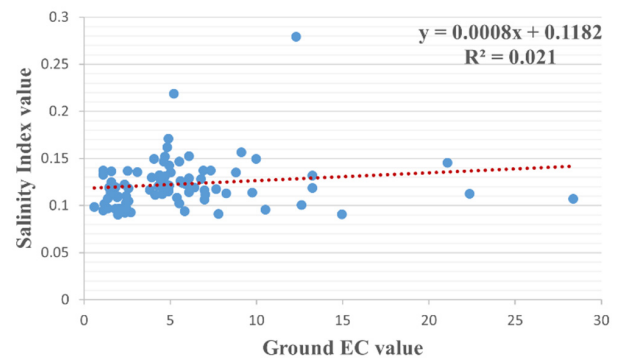


(i)

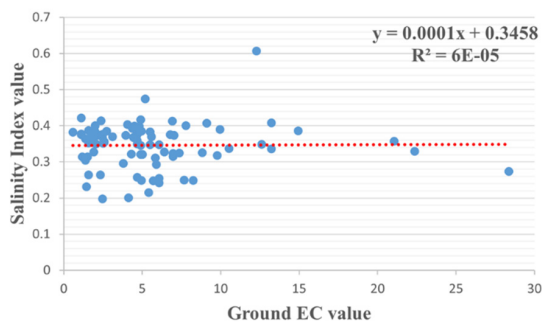
Figure 6. (a) Salinity map using salinity index 1; (b) Salinity map using salinity index 2; (c) Salinity map using salinity index 3; (d) Salinity map using salinity index 4; (e) Salinity map using salinity index 5; (f) Salinity map using salinity 6; (g) Salinity map using salinity index 7; (h) Salinity map using salinity index 8; (i) Salinity map using NDSI.



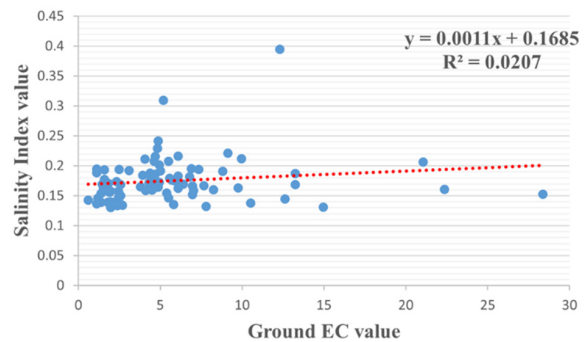
(a)



(b)



(c)



(d)

Figure 7. Cont.

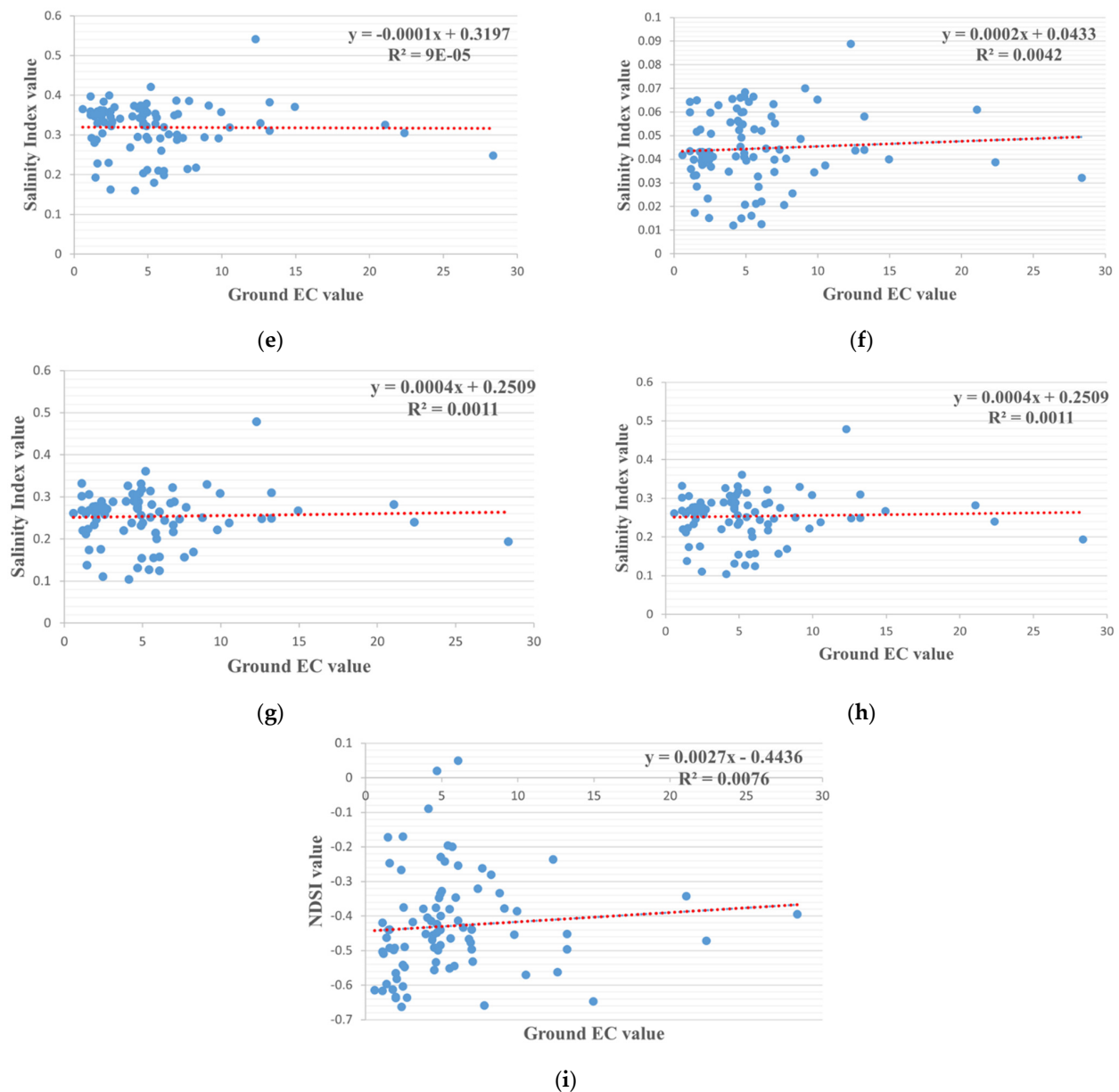


Figure 7. (a) Linear Regression between ground EC and Salinity Index 1; (b) Linear Regression between Ground EC value and Salinity Index 2; (c) Linear Regression between ground EC value and Salinity Index 3; (d) Linear Regression between Ground EC value and Salinity Index 4; (e) Linear Regression between value Ground EC value and Salinity Index 5; (f) Linear Regression between Ground EC value and Salinity Index 6; (g) Linear Regression between Ground EC value and Salinity Index 7; (h) Linear Regression between ground EC value and Salinity Index 8; (i) Linear Regression between Ground EC value and NDSI.

4. Discussion

The results of the linear regression analysis show a very negligible relationship between the satellite-based salinity indices maps and the ground truth EC values. It is observed that the maximum R^2 value for all of the salinity indices is below 0.02, and the minimum value is 0.00009, thus indicating that there is a minimal relationship between them. The linear regression analysis has been used in several case studies as a first step in creating the soil salinity maps. Researchers in El-Tina Plain, Egypt, used two predictive models, the Multivariate Adaptive Regression Splines (MARS) and the Partial Least Squares Regression (PLSR), which were based on the observed EC and the laboratory soil reflectance

spectra which were resampled, thereby resulting in Landsat sensor's resolution and R^2 values of 0.73 and 0.70 for the PLSR and MARS linear regression analyses, respectively. These results were quite good at forecasting the new EC values for various places in different years [63]. Another study in Central Iraq used the Generalized Difference Vegetation Index (GDVI) to map the soil salinity, and the authors of it found multi-temporal changes using the Landsat 4, Landsat 5, and Landsat 7 ETM+ data, thus yielding an R^2 value of 0.94. [64]. In the Lower Cliff Plain of Algeria, researchers have used five soil salinity indices comprising Landsat 7 images to detect and forecast the soil salinity: $SI\ 1 = \sqrt{B1*B3}$, $SI\ 2 = 2 * B2 - (B3 + B4)$, $SI\ 3 = \sqrt{(B2)^2 + (B3)^2}$, $SI\ 4 = (B3 - B4)/(B3+B4)$, and Soil Adjusted Salinity Index (SASI) = $B3/(100 * (B1)^2)$ [65]. They also developed a multiple linear regression model for the prediction of soil salinity based on the Soil Adjusted Salinity Index (SASI) = $B3/(100 * (B1)^2)$ and an elevation with an R^2 value of 0.45 that is between the measured EC and the predicted EC [66]. Furthermore, in a study by [42] in Tuz Lake Region, Turkey, five salinity indices were applied to Landsat 5 satellite images to monitor the soil salinization. The best result found for $SI\ 1 = \sqrt{B1*B3}$ with an R^2 value was 0.83 (Table 6). So, compared to these studies, the R^2 value that we obtained is very minimal for this study.

Table 6. Results of linear regression analysis for five different salinity indices used in the Tuz Lake Region, Turkey [42].

Salinity Index (SI)	Index Range	Sample Numbers	R^2 Value
$SI\ 1 = \sqrt{B1*B3}$	0–1	28	0.83
$SI\ 2 = \sqrt{B2*B3}$	0–1	28	0.77
$SI\ 3 = \sqrt{(B2)^2 + (B3)^2 + (B4)^2}$	0–1.73	28	0.76
$SI\ 4 = \sqrt{(B2)^2 + (B3)^2}$	0–1.42	28	0.74
$SI\ 5 = \sqrt{(B3)^2 + (B4)^2}$	0–1.42	28	0.71

On the other hand, the NDVI value that was found for the study area ranges between -0.01 and 0.48 . This low NDVI value indicates that there is a minimum amount of vegetation in the Barguna Sadar Upazila. Soil salinity might have severely affected the growth of the vegetation, and from the NDVI map, the soil of the Barguna Sadar area is severely affected by the salinity. Through the Normalized Difference Vegetation Index (NDVI), which is used to express the health of the vegetation, the remote sensing data supplied quantitative information on the status of the diverse plants. The level of plant greenness and the crop's health are related to the salinity of the soil [67–69]. The different levels of the NDVI values are linked to different soil salinity classes, for example, very severe salinization, severe salinization, moderate salinization, weak salinization, and non-salinization highlighted in Table 7.

Table 7. Hypothetical NDVI range for soil salinity levels [69].

NDVI Range	Soil Salinity Level
0.15–0.25	Very severe salinization
0.26–0.40	Moderate to Severe salinization
0.41–0.55	Moderate salinization
0.56–0.70	Weak salinization
0.71–1.00	Non-salinization

Thus, the NDVI map also visualizes the soil salinity that affects the vegetation's health. However, the regression between the soil salinity indices and the ground truth values

shows a minimum rate. As a result, it is assumed that these salinity indices do not work well to determine the soil salinity using the satellite data in the coastal area of Bangladesh.

These indices may apply to those areas where the soil salinity is visible, meaning those areas in which salt appears on the soil surface. For example, it is observed that the salt concentration is visible in Tuz Lake, Turkey. However, the salt concentration is not visible on the soil surface of the study area. Therefore, the salt concentration in the soil particles needs a laboratory analysis to be performed in order to assess the EC value. Subsequently, these formulas are insufficient for evaluating the soil salinity based on remote sensing data alone.

5. Conclusions

Climate change has substantially affected the coastal areas of Bangladesh, where 40 million people's subsistence depends on agriculture. Soil salinity that is due to climate change prevails dominantly across the rural coastal areas, and it significantly affects the crop growth's development, ultimately negatively impacting the agricultural crop production and the food security status. It also severely impacts public health by creating a shortage of fresh drinking water. From the LULC map, it is found that approximately 50 percent of the study area is agricultural land which means that the livelihood of the inhabitants depends mainly on agriculture. Therefore, to create proper land-use planning for agricultural crop production plus to address the scarcity of fresh drinking water, salinity-affected land area identification and its monitoring are essential. Significantly, salt-affected areas, and their location, intensity, and pattern varies over time, so regular investigations are warranted. However, a salinity determination is traditionally performed by field measurements that are coupled with a laboratory analysis, which is a challenging, laborious, costly, and time-consuming task when it is performed on a large scale; as such, the use of a satellite imagery-based analysis could make the processes quicker and more cost-effective, and this should be utilized in future investigations. This research was intended to determine the soil salinity area through a remote sensing analysis using some approaches, formulas, and salinity indices that were applied in other studies in different regions of the world. However, the extracted salinity values by the indices that were used have not produced satisfactory results; the correlation (R^2 value) between the salinity indices-generated salinity map and the measured salinity values was meager. On the other hand, the Soil Resource Development Institute (SRDI)-created salinity maps clearly illustrate the various soil salinity degrees for the study area. In addition, the NDVI also showed low values, indicating that there was a poor amount of or no vegetation. Consequently, it could be inferred that poor or no vegetation levels indicate the existence of soil salinity.

We can also conclude that the salinity indices that have been applied in this research are not enough to determine the soil salinity from the Landsat imagery for the study area. The reason might lie in the type or nature of the salinity and the soil's physical and chemical properties for this specific geographic area. Therefore, the performance of collaborative work with SRDI and other government and non-government agencies, identifying the alternative options of remote/proximal sensing techniques, is essential with this particular area for assessing the soil salinity.

Author Contributions: B.H. conceived and designed the study. B.H. and H.Y. conducted the research analysis and evaluation and wrote the paper. M.J.F. gathered and co-analyzed data. All authors have read and agreed to the published version of the manuscript.

Funding: This research did not receive any specific grant from funding agencies in the public, commercial, or not-for-profit sectors.

Data Availability Statement: All data are reported in this work.

Acknowledgments: The authors are grateful for the help of the University of Tsukuba, Graduate School of Science, Technology, and Information Science, Department of Life and Environmental Sciences.

Conflicts of Interest: The authors declare no conflict of interest.

References

- Ahmad, H. Coastal Zone Management Bangladesh Coastal Zone Management Status and Future Trends. *J. Coast. Zone Manag.* **2019**, *22*, 466. [CrossRef]
- Abu, M.; Kamal, U.; Rob, K. *Delineation of the Coastal Zone*; PDO-ICZMP: Dhaka, Bangladesh, 2003.
- Rawlani, A.K.; Sovacool, B.K. Building Responsiveness to Climate Change through Community Based Adaptation in Bangladesh. *Mitig. Adapt. Strateg. Glob. Chang.* **2011**, *16*, 845–863. [CrossRef]
- Catenazzo, G.; Urso, J.D.; Fragnière, E.; Tuberosa, J. *Climate Change and the Sustainable Use of Water Resources*; Springer Nature: Basel, Switzerland, 2012; pp. 499–513. [CrossRef]
- CIESIN. Low-Elevation Coastal Zone (LECZ) Rural-Urban Estimates. 2010. Available online: <http://sedac.ciesin.columbia.edu/gpw/lecz.jsp> (accessed on 10 June 2015).
- Wheeler, D. Quantifying Vulnerability to Climate Change: Implications for Adaptation Assistance. *SSRN Electron. J.* **2012**. [CrossRef]
- Rahmstorf, S. A Semi-Empirical Approach to Projecting Future Sea-Level Rise. *Science* **2007**, *315*, 368–370. [CrossRef] [PubMed]
- Pfeffer, W.T.; Harper, J.T.; O’Neel, S. Kinematic Constraints on Glacier Contributions to 21st-Century Sea-Level Rise. *Science* **2008**, *321*, 1340–1343. [CrossRef] [PubMed]
- Dasgupta, S.; Laplante, B.; Meisner, C.; Wheeler, D.; Yan, J. The Impact of Sea Level Rise on Developing Countries: A Comparative Analysis. *Clim. Change* **2009**, *93*, 379–388. [CrossRef]
- Vermeer, M.; Rahmstorf, S. Global Sea Level Linked to Global Temperature. *Proc. Natl. Acad. Sci. USA* **2009**, *106*, 21527–21532. [CrossRef] [PubMed]
- Hansen, J.E.; Sato, M. *Paleoclimate Implications for Human-Made Climate Change (2012)*; Springer: Vienna, Austria, 2011.
- Brecht, H.; Dasgupta, S.; Laplante, B.; Murray, S.; Wheeler, D. Sea-Level Rise and Storm Surges: High Stakes for a Small Number of Developing Countries. *J. Environ. Dev.* **2012**, *21*, 120–138. [CrossRef]
- Clarke, D.; Williams, S.; Jahiruddin, M.; Parks, K.; Salehin, M. Projections of On-Farm Salinity in Coastal Bangladesh. *Environ. Sci. Process. Impacts* **2015**, *17*, 1127–1136. [CrossRef]
- Solutions, S.; World, C. 19th World Congress of Soil Science Global Changes and Soil Salination Table of Contents. 2010. Available online: <https://www.iuss.org/19th%20WCSS/Symposium/pdf/WG3.4.pdf> (accessed on 8 October 2022).
- Dasgupta, S.; Hossain, M.; Huq, M.; Wheeler, D. Climate Change, Soil Salinity, and the Economics of High-Yield Rice Production in Coastal Bangladesh. *World Bank Policy Res. Work. Pap.* **2014**, 7140.
- Hossen, B.; Yabar, H.; Mizunoya, T. Land Suitability Assessment for Pulse (Green Gram) Production through Remote Sensing, GIS and Multicriteria Analysis in the Coastal Region of Bangladesh. *Sustainability* **2021**, *13*, 12360. [CrossRef]
- Dasgupta, S.; Kamal, F.A.; Khan, Z.H.; Choudhury, S.; Nishat, A. River Salinity and Climate Change: Evidence from Coastal Bangladesh. *World Sci. Ref. Asia World Econ.* **2015**, 205–242. [CrossRef]
- Haque, S.A. Salinity Problems and Crop Production in Coastal Regions of Bangladesh. *Pakistan J. Bot.* **2006**, *38*, 1359–1365.
- Rahman, S. Coastal Community Resilience to Tsunami: A Study on Planning Capacity and Social Capacity, Dichato, Chile. *IOSR J. Humanit. Soc. Sci.* **2013**, *12*, 55–63. [CrossRef]
- Dasgupta, S.; Sobhan, I.; Wheeler, D. The Impact of Climate Change and Aquatic Salinization on Mangrove Species in the Bangladesh Sundarbans. *Ambio* **2017**, *46*, 680–694. [CrossRef]
- Choudhury, S.; Dasgupta, S.; Kamal, F.A.; Khan, Z.H.; Nishat, A. *River Salinity and Climate Change: Evidence from Coastal Bangladesh (English)*; Policy Research Working Paper; World Bank Group: Washington, DC, USA, 2014; p. 6817. Available online: <https://documents.worldbank.org/curated/en/522091468209055387/River-salinity-and-climate-change-evidence-from-coastal-Bangladesh> (accessed on 9 February 2022).
- Land and Soil Resource Utilization Guide*; Soil Resource Development Institute (SRDI), SRMAF Project; Ministry of Agriculture: Dhaka, Bangladesh, 2010; pp. 3–5.
- Munns, R.; Husain, S.; Rivelli, A.R.; James, R.A.; Condon, A.T.; Lindsay, M.P.; Hare, R.A. Avenues for increasing salt tolerance of crops, and the role of physiologically based selection traits. In *Progress in Plant Nutrition: Plenary Lectures of the XIV International Plant Nutrition Colloquium*; Springer: Dordrecht, The Netherlands, 2002; pp. 93–105.
- Läuchli, A.; Grattan, S.R. *Plant Responses to Saline and Sodic Conditions*; American Society of Civil Engineers: Reston, VA, USA, 2011. [CrossRef]
- Munns, R.; Tester, M. Mechanisms of salinity tolerance. *Ann. Rev. Plant Biol.* **2008**, *59*, 651–681. [CrossRef]
- Munns, R.; Schachtman, D.P.; Condon, A.G. The significance of a two-phase growth response to salinity in wheat and barley. *Funct. Plant Biol.* **1995**, *22*, 561–569. [CrossRef]
- Flexas, J.; Diaz-Espejo, A.; Galmés, J.; Kaldenhoff, R.; Medrano, H.; Ribas-Carbo, M. Rapid Variations of Mesophyll Conductance in Response to Changes in CO₂ Concentration around Leaves. *Plant Cell Environ.* **2007**, *30*, 1284–1298. [CrossRef]
- Delfine, S.; Alvino, A.; Villani, M.C.; Loreto, F. Restrictions to Carbon Dioxide Conductance and Photosynthesis in Spinach Leaves Recovering from Salt Stress. *Plant Physiol.* **1999**, *119*, 1101–1106. [CrossRef]
- Ashraf, M.; Harris, P.J.C. Photosynthesis under Stressful Environments: An Overview. *Photosynthetica* **2013**, *51*, 163–190. [CrossRef]
- Yeo, A.R. Salinity. In *Plant Solute Transport*; Yeo, A.R., Flowers, T.J., Eds.; Blackwell: Oxford, UK, 2007; pp. 340–365.

31. Ghabour, T.; Daels, L. Mapping and Monitoring of Soil Salinity of ISSN. *Egypt. J. Soil Sci.* **1993**, *33*, 355–370.
32. Farifteh, J.; Van der Meer, F.; Atzberger, C.; Carranza, E.J.M. Quantitative Analysis of Salt-Affected Soil Reflectance Spectra: A Comparison of Two Adaptive Methods (PLSR and ANN). *Remote Sens. Environ.* **2007**, *110*, 59–78. [[CrossRef](#)]
33. Bierwirth, P.N.; Brodie, R.S. Gamma-Ray Remote Sensing of Aeolian Salt Sources in the Murray-Darling Basin, Australia. *Remote Sens. Environ.* **2008**, *112*, 550–559. [[CrossRef](#)]
34. Mulder, V.L.; de Bruin, S.; Schaepman, M.E.; Mayr, T.R. The Use of Remote Sensing in Soil and Terrain Mapping—A Review. *Geoderma* **2011**, *162*, 1–19. [[CrossRef](#)]
35. Taghizadeh-Mehrjardi, R.; Minasny, B.; Sarmadian, F.; Malone, B.P. Digital Mapping of Soil Salinity in Ardakan Region, Central Iran. *Geoderma* **2014**, *213*, 15–28. [[CrossRef](#)]
36. Mohamed, E.S.; Belal, A.; Saleh, A. Assessment of land degradation east of the Nile Delta, Egypt using remote sensing and GIS techniques. *Arab. J. Geosci.* **2013**, *6*, 2843–2853. [[CrossRef](#)]
37. Saleh, A.M.; Belal, A.B.; Mohamed, E.S. Land resources assessment of El-Galaba basin, South Egypt for the potentiality of agriculture expansion using remote sensing and GIS techniques. *Egypt. J. Rem. Sens. Space Sci.* **2015**, *18*, S19–S30. [[CrossRef](#)]
38. Saleh, A.M.; Belal, A.B.; Mohamed, E.S. Mapping of soil salinity using electromagnetic induction: A case study of East Nile Delta. *Egypt. J. Soil Sci.* **2017**, *57*, 167–174.
39. Morshed, M.M.; Islam, M.T.; Jamil, R. Soil Salinity Detection from Satellite Image Analysis: An Integrated Approach of Salinity Indices and Field Data. *Environ. Monit. Assess.* **2016**, *188*, 1–10. [[CrossRef](#)]
40. Alavipanah, S.K. Study of desertification and land changes of playa Damghan by using multitemporal and multispectral satellites. *Desert J.* **2004**, *9*, 144–154.
41. Yu, H.; Liu, M.; Du, B.; Wang, Z.; Hu, L.; Zhang, B. Mapping Soil Salinity/Sodicity by Using Landsat OLI Imagery and PLSR Algorithm over Semiarid West Jilin Province, China. *Sensors* **2018**, *18*, 1048. [[CrossRef](#)] [[PubMed](#)]
42. Gorji, T.; Sertel, E.; Tanik, A. Monitoring soil salinity via remote sensing technology under data scarce conditions: A case study from Turkey. *Ecol. Indic.* **2017**, *74*, 384–391. [[CrossRef](#)]
43. Chi, Y.; Shi, H.; Zheng, W.; Sun, J. Simulating Spatial Distribution of Coastal Soil Carbon Content Using a Comprehensive Land Surface Factor System Based on Remote Sensing. *Sci. Total Environ.* **2018**, *628–629*, 384–399. [[CrossRef](#)] [[PubMed](#)]
44. Chi, Y.; Sun, J.; Liu, W.; Wang, J.; Zhao, M. Mapping Coastal Wetland Soil Salinity in Different Seasons Using an Improved Comprehensive Land Surface Factor System. *Ecol. Indic.* **2019**, *107*, 105517. [[CrossRef](#)]
45. Tamiminia, H.; Salehi, B.; Mahdianpari, M.; Quackenbush, L.; Adeli, S.; Brisco, B. Google Earth Engine for geo-big data applications: A meta-analysis and systematic review. *ISPRS J. Photogramm. Remote Sens.* **2020**, *164*, 152–170.
46. Kumar, L.; Mutanga, O. Remote Sensing of Above-Ground Biomass. *Remote Sens.* **2017**, *9*, 935. [[CrossRef](#)]
47. Bannari, A.; Morin, D.; Bonn, F.; Huete, A. A review of vegetation indices. *Remote Sens. Rev.* **1995**, *13*, 95–120. [[CrossRef](#)]
48. Pettorelli, N.; Vik, J.O.; Mysterud, A.; Gaillard, J.M.; Tucker, C.J.; Stenseth, N.C. Using the Satellite-Derived NDVI to Assess Ecological Responses to Environmental Change. *Trends Ecol. Evol.* **2005**, *20*, 503–510. [[CrossRef](#)]
49. Pastor-Guzman, J.; Atkinson, P.M.; Dash, J.; Rioja-Nieto, R. Spatiotemporal Variation in Mangrove Chlorophyll Concentration Using Landsat 8. *Remote Sens.* **2015**, *7*, 14530–14558. [[CrossRef](#)]
50. Zhu, X.; Liu, D. Improving Forest Aboveground Biomass Estimation Using Seasonal Landsat NDVI Time-Series. *ISPRS J. Photogramm. Remote Sens.* **2015**, *102*, 222–231. [[CrossRef](#)]
51. Tian, J.; Wang, L.; Li, X.; Gong, H.; Shi, C.; Zhong, R.; Liu, X. Comparison of UAV and WorldView-2 Imagery for Mapping Leaf Area Index of Mangrove Forest. *Int. J. Appl. Earth Obs. Geoinf.* **2017**, *61*, 22–31. [[CrossRef](#)]
52. Vicente-Serrano, S.M.; Camarero, J.J.; Olano, J.M.; Martín-Hernández, N.; Peña-Gallardo, M.; Tomás-Burguera, M.; Gazol, A.; Azorin-Molina, C.; Bhuyan, U.; El Kenawy, A. Diverse Relationships between Forest Growth and the Normalized Difference Vegetation Index at a Global Scale. *Remote Sens. Environ.* **2016**, *187*, 14–29. [[CrossRef](#)]
53. Chávez, R.O.; Clevers, J.G.P.W.; Decuyper, M.; de Bruin, S.; Herold, M. 50 Years of Water Extraction in the Pampa Del Tamarugal Basin: Can Prosopis Tamarugo Trees Survive in the Hyper-Arid Atacama Desert (Northern Chile)? *J. Arid Environ.* **2016**, *124*, 292–303. [[CrossRef](#)]
54. Dutrieux, L.P.; Verbesselt, J.; Kooistra, L.; Herold, M. Monitoring Forest Cover Loss Using Multiple Data Streams, a Case Study of a Tropical Dry Forest in Bolivia. *ISPRS J. Photogramm. Remote Sens.* **2015**, *107*, 112–125. [[CrossRef](#)]
55. Abdullah, A.Y.M.; Masrur, A.; Adnan, M.S.G.; Baky, M.; Al, A.; Hassan, Q.K.; Dewan, A. Spatio-temporal patterns of land use/land cover change in the heterogeneous coastal region of Bangladesh between 1990 and 2017. *Remote Sens.* **2019**, *11*, 790. [[CrossRef](#)]
56. Tempfli, K.; Kerle, N.; Huurneman, G.C.; Janssen, L.L.F.; Bakker, W.H.; Feringa, W.; Woldai, T. *Principles of Remote Sensing, An Introductory Textbook, the International Institute for Geo-information Science and Earth Observation*; University of Twente Faculty of Geo-Information and Earth Observation (ITC): Enschede, The Netherlands, 2009; Chapter 2.2–2.4; pp. 56–85.
57. Liang, S.; Fang, H.; Chen, M. Atmospheric Correction of Landsat ETM+ Land Surface Imagery-Part I: Methods. *IEEE Trans. Geosci. Remote Sens.* **2001**, *39*, 2490–2498. [[CrossRef](#)]
58. Brown, J.W.; Hayward, H.E.; Richards, A.; Bernstein, L.; Hatcher, J.T.; Reeve, R.C.; Richards, L.A. *Diagnosis and Improvement of Saline and Alkali Soils*, 60; United States Department of Agriculture, Agriculture Handbook, 1954. Available online: https://www.ars.usda.gov/ARSUserFiles/20360500/hb60_pdf/hb60complete.pdf (accessed on 8 October 2022).

59. Khan, N.M.; Rastoskuev, V.V.; Sato, Y.; Shiozawa, S. Assessment of Hydrosaline Land Degradation by Using a Simple Approach of Remote Sensing Indicators. In *Agricultural Water Management*; Elsevier: Amsterdam, The Netherlands, 2005; Volume 77, pp. 96–109. [[CrossRef](#)]
60. Douaoui, A.E.K.; Nicolas, H.; Walter, C. Detecting Salinity Hazards within a Semiarid Context by Means of Combining Soil and Remote-Sensing Data. *Geoderma* **2006**, *134*, 217–230. [[CrossRef](#)]
61. Bannari, A.; Guedon, A.M.; El-Harti, A.; Cherkaoui, F.Z.; El-Ghmari, A. Characterization of Slightly and Moderately Saline and Sodic Soils in Irrigated Agricultural Land Using Simulated Data of Advanced Land Imaging (EO-1) Sensor. *Commun. Soil Sci. Plant Anal.* **2008**, *39*, 2795–2811. [[CrossRef](#)]
62. Abbas, A.; Khan, S. Using Remote Sensing Techniques for Appraisal of Irrigated Soil Salinity. In *Proceedings of the Land, Water & Environmental Management: Integrated Systems for Sustainability*, Christchurch, New Zealand; 2007; pp. 2632–2638. Available online: <https://researchoutput.csu.edu.au/ws/portalfiles/portal/9629947/CSU290411.pdf> (accessed on 8 October 2022).
63. Nawar, S.; Buddenbaum, H.; Hill, J.; Kozak, J. Modeling and Mapping of Soil Salinity with Reflectance Spectroscopy and Landsat Data Using Two Quantitative Methods (PLSR and MARS). *Remote Sens.* **2014**, *6*, 10813–10834. [[CrossRef](#)]
64. Wu, W.; Mhaimeed, A.S.; Al-Shafie, W.M.; Ziadat, F.; Dhehibi, B.; Nangia, V.; De Pauw, E. Mapping Soil Salinity Changes Using Remote Sensing in Central Iraq. *Geoderma Reg.* **2014**, *2–3*, 21–31. [[CrossRef](#)]
65. Yahiaoui, I.; Douaoui, A.; Zhang, Q.; Ziane, A. Soil Salinity Prediction in the Lower Cheliff Plain (Algeria) Based on Remote Sensing and Topographic Feature Analysis. *J. Arid Land* **2015**, *7*, 794–805. [[CrossRef](#)]
66. Zhang, T.T.; Qi, J.G.; Gao, Y.; Ouyang, Z.T.; Zeng, S.L.; Zhao, B. Detecting Soil Salinity with MODIS Time Series VI Data. *Ecol. Indic.* **2015**, *52*, 480–489. [[CrossRef](#)]
67. Shrestha, R.P. Relating Soil Electrical Conductivity to Remote Sensing and Other Soil Properties for Assessing Soil Salinity in Northeast Thailand. *L. Degrad. Dev.* **2006**, *17*, 677–689. [[CrossRef](#)]
68. Jiapaer, G.; Chen, X.; Bao, A. A Comparison of Methods for Estimating Fractional Vegetation Cover in Arid Regions. *Agric. For. Meteorol.* **2011**, *151*, 1698–1710. [[CrossRef](#)]
69. Djuraev, A.; Mirdjalalov, D.; Nuratdinov, A.; Khushvaktov, T.; Karimov, Y. Evaluation of Soil Salinity Level through NDVI in Syrdarya Province, Uzbekistan. *E3S Web Conf.* **2021**, *258*, 03017. [[CrossRef](#)]